Performance of Whole-Body Integrated ^{18}F-FDG PET/MR in Comparison to PET/CT for Evaluation of Malignant Bone Lesions

Matthias Eiber*[1], Toshiki Takei*[2], Michael Souvatzoglou[2], Marius E. Mayerhoefer[3], Sebastian Fürst[2], Florian C. Gaertner[2], Denys J. Loeffelbein[4], Ernst J. Rummeny[1], Sibylle I. Ziegler[2], Markus Schwaiger[2], and Ambros J. Beer[2]

[1]*Department of Radiology, Technische Universität München, Klinikum rechts der Isar, Munich, Germany;* [2]*Department of Nuclear Medicine, Technische Universität München, Klinikum rechts der Isar, Munich, Germany;* [3]*Department of Radiology and Nuclear Medicine, Medical University of Vienna, Vienna, Austria; and* [4]*Department of Oral and Maxillofacial Surgery, Technische Universität München, Klinikum rechts der Isar, Munich, Germany*

Because of its higher soft-tissue contrast, whole-body integrated PET/MR offers potential advantages over PET/CT for evaluation of bone lesions. However, unlike PET/CT, PET/MR ignores the contribution of cortical bone in the attenuation map. Thus, the aims of this study were to evaluate the diagnostic performance of whole-body integrated ^{18}F-FDG PET/MR specifically for bone lesions and to analyze differences in standardized uptake value (SUV) quantification between PET/MR and PET/CT. **Methods:** One hundred nineteen patients with ^{18}F-FDG–avid primary malignancies underwent a single-injection, dual-imaging protocol using ^{18}F-FDG on a PET/CT scanner and a subsequent PET/MR scan with a T1-weighted volumetric interpolated breath-hold examination (VIBE) Dixon sequence for attenuation correction and an unenhanced coronal T1-weighted turbo spin-echo (TSE) sequence for bone analysis. Three sets of images (CT with PET [from PET/CT; set A], T1-weighted VIBE Dixon with PET [set B], and T1-weighted TSE with PET [both from PET/MR; set C]) were analyzed. Two readers rated every lesion using a 4-point scale for lesion conspicuity on PET, a 4-point scale for anatomic allocation of PET-positive lesions, and a 5-point scale for the nature of every lesion based on its appearance on morphologic imaging and uptake on PET. For all lesions and for representative regions of normal bone, SUV analysis was performed for PET/MR and PET/CT. **Results:** In total, 98 bone lesions were identified in 33 of 119 patients, and 630 regions of normal bone were analyzed. Visual lesion conspicuity on PET was comparable for PET/CT (mean rating, 2.82 ± 0.45) and PET/MR (2.75 ± 0.51; $P = 0.3095$). Anatomic delineation and allocation of suggestive lesions was significantly superior with T1-weighted TSE MRI (mean rating, 2.84 ± 0.42) compared with CT (2.57 ± 0.54, $P = 0.0001$) or T1-weighted VIBE Dixon MRI (2.57 ± 0.54, $P = 0.0002$). No significant difference in correct classification of malignant bone lesions was found among sets A (85/90), B (84/90), and C (86/90). For bone lesions and regions of normal bone, a highly significant correlation existed between the mean SUVs for PET/MR and PET/CT ($R = 0.950$ and 0.917, respectively, each $P < 0.001$). However, substantially lower mean SUVs were found for PET/MR than for PET/CT both for bone lesions (12.4% ± 15.5%) and for regions of normal bone (30.1% ± 27.5%). **Conclusion:** Compared with PET/CT, fully integrated whole-body ^{18}F-FDG PET/MR is technically and clinically robust for evaluation of bone lesions despite differences in attenuation correction. PET/MR, including diagnostic T1-weighted TSE sequences, was superior to PET/CT for anatomic delineation and allocation of bone lesions. This finding might be of clinical relevance in selected cases—for example, primary bone tumors, early bone marrow infiltration, and tumors with low uptake on PET. Thus, a diagnostic T1-weighted TSE sequence is recommended as a routine protocol for oncologic PET/MR.

Key Words: hybrid imaging; PET/CT; PET/MR; bone lesion; SUV; detection

J Nucl Med 2014; 55:191–197
DOI: 10.2967/jnumed.113.123646

The recent introduction of PET/MR scanners goes along with high expectations of a new, powerful multimodality imaging tool (*1–4*). The skeletal system is frequently involved in metastatic disease, and early detection of bone metastases has an important impact on patient management, disease outcome, and quality of life (*5*). For bone lesions, the higher soft-tissue contrast of MR has proven to be more sensitive than CT for the early detection of bone marrow pathologies (*6,7*). Thus, PET/MR is expected to yield advantages for detecting and delineating bone metastases and primary bone tumors.

First data using a whole-body fully integrated PET/MR scanner indicated that the performance of PET with this system is generally equivalent to PET/CT (*2*). However, these initial results were not focused specifically on bone lesions. Moreover, the results of this former study were based on the comparison of low-dose CT and a low-resolution T1-weighted Dixon volumetric interpolated breath-hold examination (VIBE) sequence used for attenuation correction. However, in clinical practice, radiologists mainly use T1-weighted spin-echo sequences to demonstrate the replacement of fatty marrow by infiltration of tumor cells (*8,9*). T1-weighted spin-echo sequences usually have a higher in-plane resolution and provide a better visualization of bone marrow and bone lesions than the T1-weighted Dixon VIBE sequence used for attenuation correction in PET/MR.

Received Mar. 26, 2013; revision accepted Aug. 14, 2013.
For correspondence or reprints contact: Matthias Eiber, Klinikum rechts der Isar der TUM, Department of Radiology, Ismaninger Strasse 22, 81675 Munich, Germany.
E-mail: matthias.eiber@tum.de
*Contributed equally to this work.
Published online Dec. 5, 2013.

In addition, quantitative analysis of tracer uptake using the standardized uptake value (SUV) is essential for correct analysis of PET tracer distribution (e.g., for follow-up studies and for assessing response). In contrast to CT data, which can easily be transformed into attenuation coefficients for PET, intensity values in MR images do not reflect the x-ray density of tissues (*10*). Different approaches have been described, including tissue segmentation, the use of atlases or templates, pattern recognition techniques, or a combination of these (*11–13*). In the commercially available whole-body fully integrated PET/MR system, only a 2-point Dixon-based MR sequence is currently approved by the Food and Drug Administration for attenuation correction. This approach neglects the contribution of bone signal (*14*). However, there are no convincing clinical data showing whether it is necessary to additionally segment bone in MR attenuation correction maps or whether it is clinically acceptable to replace the stronger attenuation of the 511-keV photons of bone by the attenuation of soft tissue.

Thus, the purpose of our study was 2-fold. The first purpose was to evaluate the potential of PET/MR, including diagnostic MR sequences for detecting and delineating bone lesions, compared with PET/CT, in patients with oncologic diseases. The second was to analyze the significance of neglecting the contribution of bone in Dixon-based attenuation correction in PET/MR, compared with PET/CT.

MATERIALS AND METHODS

Patient Characteristics

In a retrospective analysis, all patients who underwent a dual-imaging, single-injection protocol consisting of ^{18}F-FDG PET/CT and subsequent PET/MR with the smallest possible temporal delay were retrieved from the institutional database. Only patients with a history or suspicion of an oncologic disease and the acquisition of unenhanced T1-weighted turbo spin-echo (TSE) sequences on PET/MR were included. The institutional review board approved the study, and all subjects signed an informed consent form. Exclusion criteria were pregnancy, standard contraindications for MR imaging examinations, and inability to undergo a second examination after the PET/CT scan. In pediatric patients, the clinical necessity of whole-body MR imaging served as an additional precondition for the PET/MR scan, which then replaced standalone whole-body MR imaging.

A total of 119 patients (54 female and 65 male) with a mean age of 53.4 y (range, 7–86 y) were included in the study. Indications for referral are illustrated in Table 1. The mean injected activity of ^{18}F-FDG was 382 MBq (range, 193–504 MBq [adjusted for body weight]; SD, 53.6 MBq). Patients fasted 6 h before tracer injection, and blood glucose levels were measured just before injection, with a cutoff of 150 mg/dL.

PET/CT Acquisition

PET/CT scans were acquired on a Biograph Sensation 64 PET/CT scanner (Siemens Healthcare). For attenuation correction purposes and anatomic correlation, a low-dose CT scan (120 keV, 20 mAs, no intravenous contrast material) was acquired in resting expiratory position. All patients received oral contrast material (Telebrix; Guerbet), 15 mL diluted in 1 L of water. When clinically indicated, a dedicated CT scan was obtained (120 kV, 240 mAs, 0.5 s per rotation, 5-mm slice thickness, portal venous phase 80 s after the injection of 80–120 mL of intravenous contrast agent [Iomeron 300; Bracco]). In patients with a diagnostic CT scan, this scan was used for attenuation correction. PET/CT acquisition was started at a mean of 87.6 min after tracer injection (SD, 25.1 min; range, 59–123 min). Emission time was 2–3 min per bed position, with 5–6 bed positions per patient (head to pelvis).

TABLE 1
Indication for Referrals

Malignancy	All patients (n = 119)	Patients suitable for SUV measurement (n = 84)
Head and neck squamous cell carcinoma	20	20
Breast cancer	19	9
Gastrointestinal tract cancer	17	12
Sarcoma	15	13
Malignant lymphoma/ leukemia	11	6
Primary unknown cancer	10	4
Genitourinary cancer	9	8
Malignant melanoma	9	5
Thyroid cancer	7	7
Lung	3	—
Other	4	3
Total	125*	87†

*6 patients had history of 2 primary tumors.
†3 patients had history of 2 primary tumors.

PET/MR Acquisition

PET/MR was performed on a fully integrated whole-body hybrid system (Biograph mMR; Siemens Healthcare). A detailed summary was recently published of the scanner's technical specifications and performance, as well as a comparison of the basic specifications of the PET components between the Biograph Sensation 64 and the Biograph mMR (*2,15*). PET/MR was acquired at a mean of 137.2 min after tracer injection (SD, 25.8 min; range, 47–159 min). Thus, on average the time difference between the start of the 2 examinations was 49.6 min. Because of workflow considerations, in 3 patients PET/MR was acquired before PET/CT. When these 3 patients are excluded, the mean time difference between the start of the 2 examinations was 54.1 min.

The PET/MR acquisition protocol was as follows. First, MR sequences were acquired to determine the location and number of PET bed positions. Then, the PET emission scans were initiated, with an emission time of 4 min per bed position. Simultaneously with the PET measurements, a 2-point T1-weighted coronal 3-dimensional VIBE sequence was acquired for attenuation correction purposes. A centric k-space acquisition was chosen to minimize motion artifacts from incomplete breath-holds (*16*). From the raw images, 4 different images were created: in-phase, opposed-phase, water-weighted, and fat-weighted. In addition, all patients underwent a coronal T1-weighted TSE sequence. The technical parameters are included in Table 2.

Image Reconstruction

To maintain comparability, similar reconstruction methods were used for the PET data acquired on the PET/CT and PET/MR scanners. Details on reconstruction of the PET data for PET/CT and PET/MR, including the use of the T1-weighted VIBE Dixon for attenuation correction, have been published recently (*2*). All images were uploaded to a dedicated workstation (Syngo MMWP; Siemens Healthcare).

TABLE 2
Technical Parameters of Different MR Sequences Used in Study

Sequence	T1-weighted VIBE Dixon	T1-weighted TSE coronal
TR/TE (ms)	3.60/1.23–2.46*	600/8.7
Slice thickness (mm)	3.12	5
Gap (%)	0	30
Matrix	192 × 121	384 × 230
Field of view (mm)	500	450
% phase field of view	100	67.2
Acquisition time (min:s)	0:19	1:11
Number of excitations	1	1
iPAT factor	2	2

*Fat-saturation techniques with Dixon require 2 repetition times.

TR/TE = repetition time/echo time; iPAT = integrated parallel acquisition technique.

Image Analysis

Lesion Detection, Delineation, and Characterization. Image datasets from PET/CT and PET/MR were divided into 3 subsets: CT together with PET from PET/CT (set A), T1-weighted Dixon in-phase images together with PET from PET/MR (set B), and T1-weighted TSE images together with PET from PET/MR (set C). These sets were analyzed by 2 experienced readers (1 board-certified nuclear medicine physician and 1 board-certified radiologist) in consensus without knowledge of the patient history.

To avoid any learning bias, the sets were analyzed in random order at an interval of 4 wk in the following manner. For every set, primarily the PET images were analyzed with the corresponding morphologic dataset and every suggestive lesion was noted. The conspicuity of all lesions in the PET dataset was rated on a 4-point scale, with 0 indicating no uptake on PET (in the case of a PET-negative lesion); 1, low uptake (less than liver); 2, moderate uptake (comparable to liver); and 3, high uptake (more than liver). The anatomic delineation of every PET-positive lesion was scored on a 4-point scale, with 1 indicating no anatomic allocation possible; 2, questionable anatomic allocation; 3, good anatomic allocation without a clear morphologic correlate; and 4, excellent anatomic allocation with a clear morphologic correlate. The nature of every lesion based on its appearance on morphologic imaging and uptake on PET was rated on a 5-point scale, with 1 indicating definitely malignant; 2, probably malignant; 3, indeterminate; 4, probably benign; and 5, definitely benign. A maximum of 5 lesions per patient was analyzed to avoid bias from patients with a very high number of lesions. Follow-up examinations or clinical data served as a standard of reference.

Quantitative Comparison of SUVs. SUVs were analyzed as previously published (*2*). All ^{18}F-FDG–positive lesions determined in the prior analysis and representative regions of normal bone were analyzed. For technical reasons concerning scanner software development and slight changes in the μ map, the SUVs of patients scanned before June 2011 were not directly comparable to those of patients scanned after this date. However, there is no subjective difference with regard to visual analysis. The following attenuation factors were implemented in the latest version: background, 0 cm^{-1}; lung, 0.0224 cm^{-1}; fat, 0.0854 cm^{-1}; and soft tissue, 0.1000 cm^{-1}. In consequence, SUV measurements were obtained for all (n = 84) patients whose scans were obtained since June 2011 (Table 1). To avoid overrating of individual patients, we limited the number of rated lesions to 5 per patient.

For all ^{18}F-FDG–positive lesions, 1 board-certified nuclear medicine physician placed regions of interest with an isocontour of 50% around the mean SUV (SUV_{mean}) and maximum SUV (SUV_{max}) for PET/CT and PET/MR. The dedicated Syngo MMWP workstation allows visually controlled automatic coregistration of different datasets from 1 patient. In addition, a region of interest was placed on CT images and the mean Hounsfield unit was measured. Lesions on CT were categorized as lytic (<100 Hounsfield units), mixed (100–300 Hounsfield units), or sclerotic (>300 Hounsfield units).

For regions of normal (nonpathologic) bone, regions of interest in 3 consecutive anatomically corresponding central axial slices delineating the shape of the organ but not including edge pixels were drawn, and the SUV_{mean} and SUV_{max} were noted. Depending on the scan range, which was covered both in PET/CT and PET/MR, the following regions were analyzed: pelvis, proximal femur, and humerus bilaterally; sacral bone; and cervical, thoracic, and lumbar spine.

Statistical Analysis

Statistical analysis was performed using the MedCalc 12.3.0.0 software package for Windows. P values of less than 0.05 were considered statistically significant. To analyze the diagnostic performance of both modalities, the detection rate was calculated on the basis of the total number of malignant lesions determined by the standard of reference. The Fisher exact test was used to analyze agreement on the number of detected lesions between PET/CT and PET/MR and the possible difference in assessing malignant lesions. For calculating correlations between the SUVs derived from PET/MR and PET/CT, the Spearman rank correlation coefficient was used. The overall

TABLE 3
Quality of Anatomic Location and Delineation of Suggestive Lesions

Location	n	Lytic/mixed/sclerotic	CT	Dixon	T1-weighted TSE
Cervical spine	4	1/3/0	2.00 ± 0.82	2.25 ± 0.50	3.00*
Thoracic spine	16	0/15/1	2.50 ± 0.52	2.81 ± 0.40	2.94 ± 0.25
Lumbar spine	20	3/14/3	2.60 ± 0.51	2.70 ± 0.47	3.00*
Pelvis	27	5/13/9	2.59 ± 0.51	2.76 ± 0.55	2.85 ± 0.36
Upper extremity or shoulder	12	1/10/1	2.75 ± 0.45	2.58 ± 0.52	2.92 ± 0.29
Legs	6	1/4/1	2.50 ± 0.84	2.66 ± 0.82	2.67 ± 0.82
Ribs or sternum	11	2/6/3	2.63 ± 0.51	1.72 ± 0.79	2.36 ± 0.67
Other	2	0/1/1	2.50 ± 0.71	1.50 ± 0.71	2.50 ± 0.71
Total	98	13/66/19	2.57 ± 0.54	2.54 ± 0.65	2.84 ± 0.42

*Same results for all lesions, SD = 0.

Data are mean ± SD.

statistical differences in measured SUVs were tested using the nonparametric Wilcoxon matched-pairs signed rank test. Because a high degree of correlation does not necessarily imply good agreement between the 2 measurements, a Bland–Altman plot was constructed to assess this agreement (*17*). A Bland–Altman plot displays the difference between the 2 measurements versus their average as a scatterplot, on which each point represents 1 measurement.

RESULTS

Visual Analysis

Lesion Detection, Location, and Delineation. Thirty-three of 119 patients showed conspicuous lesions, totaling 98. According to the standard of reference, 90 lesions were malignant and 8 were benign. All lesions were identified on PET/CT (set A) and on the T1-weighted TSE sequence for PET/MR (set C). The T1-weighted VIBE Dixon sequence for PET/MR (set B) missed 1 PET-negative malignant lesion in the ribs.

In rating the anatomic location and presence of a morphologic correlate, T1-weighted TSE images (mean rating, 2.84 ± 0.42) performed significantly better than CT (mean rating, 2.57 ± 0.54, $P = 0.0001$) and T1-weighted Dixon in-phase images (mean rating, 2.57 ± 0.54, $P = 0.0002$). The results for the different skeletal regions are presented in Table 3. Although not statistically significant because of low numbers, CT performed substantially better than either T1-weighted TSE or T1-weighted Dixon in-phase images for demonstrating an anatomic correlate for lesions in the ribs. In contrast, T1-weighted TSE images were substantially superior to CT and T1-weighted VIBE Dixon images for the spine (especially the cervical spine) and pelvis. Two examples are given in Figure 1 and Supplemental Figure 1 (supplemental materials are available at http://jnm.snmjournals.org).

Lesion Conspicuity on PET. In total, 85 of 98 lesions showed abnormally increased uptake on PET. The quality of visual lesion conspicuity on PET was similar for the 2 modalities, with a mean of 2.82 ± 0.45 for the PET dataset from PET/CT and 2.75 ± 0.51 for the PET dataset from PET/MR ($P = 0.3095$). An example is given in Figure 2.

Lesion Characterization. In terms of lesion characterization, no significant differences could be found between sets A, B, and C. Performance was nearly identical, as a correct classification of all malignant lesions could be found for sets A, B, and C for 85, 84, and 86, respectively of 90 lesions. In each set, the remaining malignant lesions were classified as indeterminate. A table outlining the confidence in rating the lesions is available as Supplemental Table 1. Remarkably, 6 PET-negative lesions were correctly classified as malignant bone lesions in sets A and C. Of these lesions, one was completely missed in set B but recognized in sets A and C and correctly classified as malignant. One additional PET-negative malignant lesion was recognized in set B but classified as indeterminate. Of the benign lesions noted, sets A, B, and C correctly classified 6, 7, and 8, respectively, of 8 lesions. The remaining lesions in sets A and B were classified as indeterminate.

Quantitative Comparison of SUVs

^{18}F-FDG–Positive Lesions. Eighty ^{18}F-FDG–positive osseous lesions in 25 patients could be included in the quantitative analysis. Thirty-two lesions were in the vertebral bodies of the cervical, thoracic, or lumbar spine; 18 in the pelvic bones; 9 in the ribs; 13 in the sternum, shoulder girdle, or humerus; 6 in the lower extremity; and 2 in other bones. Further analysis of the density of lesions on CT images revealed 10 nonsclerotic, 52 mixed-sclerotic, and 180 sclerotic lesions.

Overall, the SUV_{mean} and SUV_{max} obtained from PET/CT and PET/MR did correlate significantly ($R = 0.950$ and $R = 0.937$, respectively; $P < 0.0001$; Fig. 3A). However, SUV_{mean} and SUV_{max} were significantly lower in PET/MR (Table 4 provides details on SUV). A Bland–Altman plot displaying the excellent agreement but outlining the systematic difference is available as Supplemental Figure 2A.

The SUV_{mean} in bone lesions was a mean of 12.4% ± 15.5% lower for PET/MR than for PET/CT. The highest discrepancy, with a 51.5% lower SUV_{mean} for PET/MR, was for a lesion in the right proximal humerus. However, the position of this patient's arms was different between PET/MR and PET/CT (arms down in PET/MR, arms up in PET/CT), and the lesion was at the end of the field of view on the PET/MR scan. There was a tendency to a higher deviation with lower values on PET/MR for pelvic lesions (mean, −11.4% ± 17.5%), compared with lesions in the spine (mean, −9.2% ± 13.6%), although the difference was not statistically significant ($P = 0.632$). No correlation in the difference in SUV between PET/MR and PET/CT could be found depending on the density in CT ($P = 0.0037$, $R = 0.973$, Supplemental Fig. 3).

Normal Regions. Six hundred thirty regions of normal bone could be analyzed. Overall, the SUV_{mean} and SUV_{max} obtained

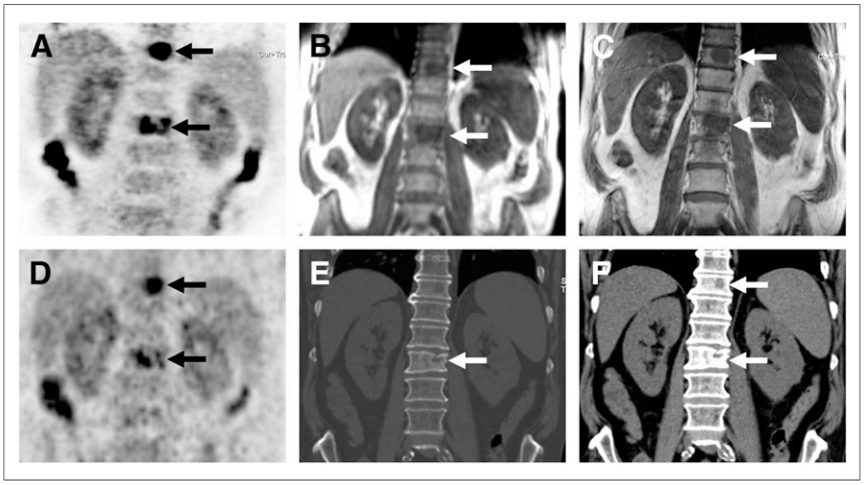

FIGURE 1. Images of bone metastases (arrows) in 69-y-old man presenting for staging of oropharyngeal cancer. (A–C) PET/MR examination with coronal PET (A), coronal T1-weighted Dixon in-phase MR sequence (B), and coronal T1-weighted TSE MR sequence (C). (D–F) PET/CT examination with coronal PET (D) and coronal bone (E) and soft-tissue (F) windows of CT dataset. Two metastases in spine show intense uptake in both PET datasets (A and D). Replacement of bone marrow is seen in both T1-weighted Dixon in-phase MR sequence (B) and T1-weighted TSE MR sequence (C), with better lesion delineation in TSE than in VIBE Dixon because of higher in-plane resolution. (E and F) Faint sclerosis is present as anatomic correlate of caudal metastases in both bone window (E) and soft-tissue window (F) on CT, whereas cranial metastasis is depicted only in soft-tissue window.

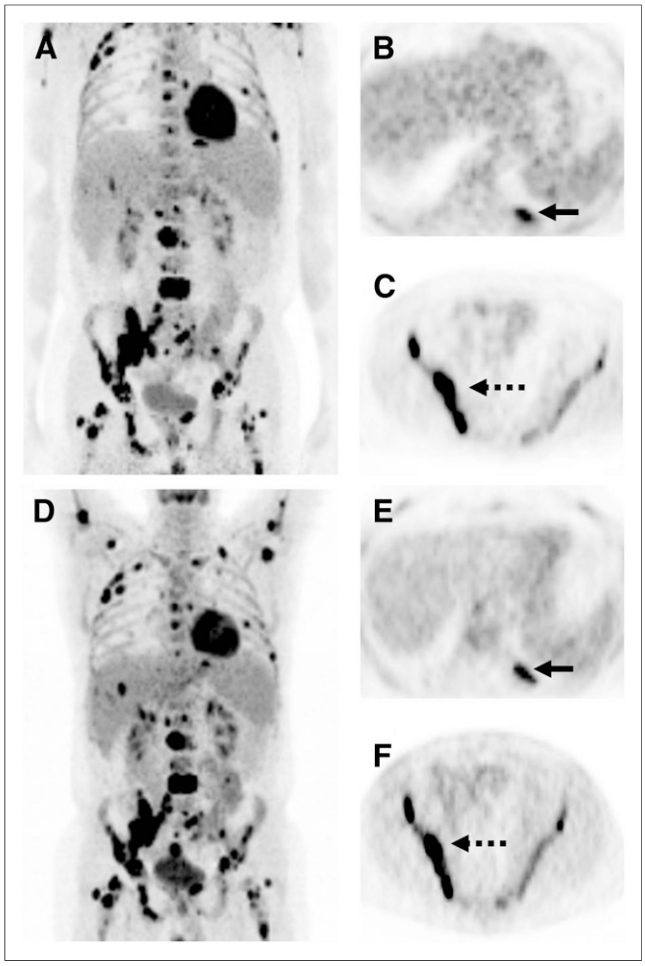

FIGURE 2. PET/MR (A–C) and PET/CT (D–F) images from patient with diffuse osseous manifestation of non-Hodgkin lymphoma. Visually, both datasets provide excellent image quality, as demonstrated by maximum-intensity projection (A and D). Patient is imaged with arms down in PET/MR (A) and arms up in PET/CT (B). This approach is often used because imaging time in PET/MR is lengthy and too uncomfortable for a patient lying with arms up. Quantitative analysis showed lower SUV_{mean} for lesions on PET/MR (121 min after injection) than on PET/CT (85 min after injection). Moderate difference (29.4%) was found for lesions in left rib (PET/MR, 5.99; PET/CT, 7.75; arrows in B and E). Slight difference (10.4%) was observed for lesion in right ilium (PET/MR, 19.86; PET/CT, 22.16; arrows in C and F).

from PET/CT and PET/MR did correlate significantly ($R = 0.917$ and $R = 0.891$, respectively; $P < 0.0001$; Fig. 3B). However, SUV_{mean} and SUV_{max} were significantly lower for PET/MR than for PET/CT (each $P < 0.0001$; Table 5). Better visualization of the excellent agreement, but again a systematic difference, is seen in the Bland–Altman plot available as Supplemental Figure 2A. The SUV_{mean} in regions with normal bone was 30.1% ± 27.5% lower for PET/MR than for PET/CT.

DISCUSSION

In this study, we have shown that the overall performance of PET/MR and PET/CT using ^{18}F-FDG was equivalent for detecting and characterizing bone lesions in ^{18}F-FDG–avid malignancies. Thus, for visual evaluation of PET-positive bone lesions, the different methods for attenuation correction are not clinically relevant. With regard to lesion delineation and anatomic allocation of PET-positive findings, PET/MR with diagnostic T1-weighted TSE sequences was superior to PET/CT and PET/MR with T1-weighted Dixon in-phase images. However, significantly lower SUVs were measured for PET/MR.

Our study showed that in terms of anatomic location and delineation of a PET-positive bone lesion, the diagnostic T1-weighted TSE MR sequence performed significantly better than either CT or the in-phase dataset of the T1-weighted VIBE Dixon sequence used for attenuation correction in PET/MR. Using a diagnostic T1-weighted TSE MR sequence for bone marrow imaging in PET/MR results in a higher number of bone lesions for which the morphologic-functional information is concordant. This concordance is expressed by a higher score in anatomic lesion delineation, which in principal could lead to a higher level of diagnostic confidence. In our study, only in 1 case did the combination of PET and T1-weighted TSE images lead to a correct classification of the lesions, compared with PET/CT. However, especially in cases of lesions with moderate or weak ^{18}F-FDG uptake, or for restaging after therapy, additional concordant information from the morphologic dataset could be advantageous. Because a wide variety of diseases and indications were included in the present study, we cannot answer this question definitely, and thus, this hypothesis has to be confirmed in future studies.

Notably, although our study showed that the anatomic location and allocation of PET-positive lesions was superior on PET/MR, it also showed that in our patient population the detection and characterization of bone lesions was overall comparable to PET/CT, as could be related to inclusion of primarily ^{18}F-FDG–avid malignancies. In such cases, the combination of PET and CT is regarded as a robust imaging modality with an already very high sensitivity (*18,19*). Compared with whole-body MR imaging, PET/CT has been shown to perform equally well or to be only slightly inferior for the detection of bone lesions (*18,19*). Consequently, the results of our study agree well with these prior studies, as they confirm that for ^{18}F-FDG–avid tumors, PET/CT has a high diagnostic accuracy that is not significantly exceeded by MR. This result, however, might be different for tumors with

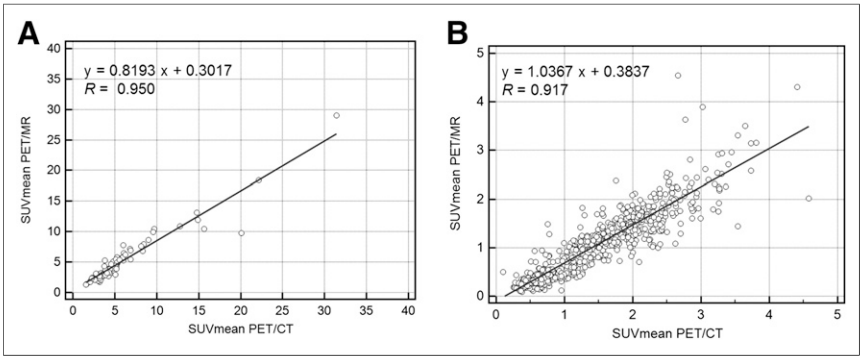

FIGURE 3. Correlation of tracer uptake between PET/CT and subsequent PET/MR as assessed by SUV_{mean}. *x*-axis displays quantitative values obtained by PET/CT, and *y*-axis displays corresponding values by PET/MR. Both for bone lesions (A) and for regions of normal bone (B), high correlation as expressed by Spearman correlation coefficient is found ($R = 0.950$ and $R = 0.917$, $P < 0.0001$, respectively) between the 2 modalities.

TABLE 4
SUV_{mean} and SUV_{max} for Bone Lesions

Technique	SUV_{mean}	SUV_{max}
PET/CT	5.70 ± 4.70	8.54 ± 6.96
PET/MR	4.97 ± 4.03	7.55 ± 6.02
P	<0.0001	<0.0001

Data are mean ± SD.

variable ^{18}F-FDG uptake or when PET/MR is used in combination with other tracers in other malignancies.

On the basis of our qualitative analysis for bone lesions, PET from PET/MR is equivalent to PET from PET/CT when the uptake is judged visually. Consequently, the attenuation correction provided by the T1-weighted VIBE Dixon sequence, which neglects the contribution of cortical bone, is adequate for clinical use. In our study, this adequacy is expressed by only slight differences in the visual lesion conspicuity between the 2 PET datasets.

Our quantitative results also show the robustness of the use of a T1-weighted VIBE Dixon sequence for attenuation correction by the high correlation between the SUVs from PET/CT and PET/MR ($P < 0.0001$). Nevertheless, in total there was a mean underestimation of 12.4% for bone lesions and 30.1% for regions of normal bone. For lesions, these differences are slightly higher than previously reported in studies simulating the attenuation correction with different approaches. In those studies, the mean underestimations were between 6.5% and 10% using a 3- or 4-tissue segmentation or by replacing all Hounsfield units greater than 100 with soft-tissue density (*12,13,20,21*). However, these were studies not using an actual PET/MR scanner but only simulation. Any simulated approach cannot completely imitate the performance of PET using a 4-tissue-class segmentation implemented in a hybrid PET/MR scanner (e.g., disregard of scanner geometry and potential discrepancies in patient positioning). These technical issues could be the source of the single high differences between the SUVs (≤51.5% in our study). Nevertheless, another study using a 5-tissue segmentation approach with simulated data from PET/CT and multistation MR reported single maximum deviations for bone lesions in that range (>50%) (*11*). Finally, there are also reports (*22,23*) stating that the SUVs from bone for PET/CT might be overestimated compared with a transmission scan with an external source performed on stand-alone PET, which is still considered the standard of reference. For instance, one study showed that CT-derived μ values were 14% higher than the μ values calculated with the conventional transmission scan (*23*). The higher difference for regions of normal bone than for malignant bone lesions in our study fits well with the observation by Kumar et al. of a decrease in the background SUV over time for normal bone as opposed to malignant lesions (*24*). Because we imaged the patients first on PET/CT and then on PET/MR, the difference between CT- and MR-based SUVs could potentially be even higher. However, this hypothesis has to be clarified in further investigations.

TABLE 5
SUV_{mean} and SUV_{max} for Regions of Normal Bone

Technique	SUV_{mean}	SUV_{max}
PET/CT	1.520 ± 0.658	2.300 ± 1.070
PET/MR	1.092 ± 0.705	1.820 ± 0.998
P	<0.0001	<0.0001

Data are mean ± SD.

As a corollary result of our study, there was no correlation between the degree of sclerosis and the mean underestimation for PET/MR compared with PET/CT. Though not statistically significant, a tendency for a more pronounced underestimation was reported in a recent study (*21*). Because this study was based on a simulated approach using CT data, a direct comparison is not possible.

Our study had several limitations: First, the inclusion of primarily ^{18}F-FDG–avid tumors leads to high detection rates regardless of whether PET/CT or PET/MR is used. Thus, the potential added value of the morphologic dataset (CT vs. MR) is presumably more limited than when a broader variety of tumors is included. In the detection of ^{18}F-FDG–negative lesions, the performance of the CT versus MR components might differ more considerably. Second, we did not provide a gold standard based on histopathology for the lesions included in the study. A histopathologic gold standard was not possible, particularly for ethical reasons in many cases, and was not necessary as we primarily wanted to compare the diagnostic ability of PET/MR and PET/CT based on their technical differences. For SUV measurement, differences in the quantification might also be related to differences in the position of a single lesion between PET/MR and PET/CT (e.g., different rotation of the arms).

In contrast to dedicated MR protocols, our PET/MR protocol evaluated only the performance of T1-weighted TSE images instead of additionally acquiring a T2-weighted fat-suppressed sequence. However, fat-saturated T2-weighted sequences mainly serve as a screening tool for osteolytic lesions showing high signal intensity (*6,9*), which in the case of ^{18}F-FDG–avid primary tumors often show a very high signal on PET anyway (*25,26*). Thus, ^{18}F-FDG uptake in these cases is sensitive in detecting lesions, whereas ^{18}F-FDG uptake in mainly osteosclerotic lesions can be low to moderate. Consequently, we think that the combination of PET—which is highly sensitive for osteolytic lesions—and a T1-weighted TSE MR sequence—which is sensitive for osteosclerotic lesions—is sufficient.

CONCLUSION

Neglecting the contribution of cortical bone in Dixon-based attenuation correction for integrated PET/MR is clinically not relevant for the detection of ^{18}F-FDG bone lesions. PET/MR using either a Dixon in-phase sequence or a T1-weighted TSE sequence for anatomic delineation of bone lesions performs equally as well as PET/CT; however, the higher rate of concordant findings between T1-weighted TSE images and PET compared with CT and Dixon in-phase images can potentially improve diagnostic certainty, and its inclusion in an oncologic PET/MR protocol is recommended. Because of slight differences in SUV quantification for bone lesions between PET/MR and PET/CT in cases requiring quantitative response assessment, the same scanner type should be used for sequential studies. Now, larger prospective studies possibly including both ^{18}F-FDG–avid and –negative malignancies are warranted to further evaluate the role of PET/MR for a broad variety of bone lesions, including ^{18}F-FDG–negative tumors.

DISCLOSURE

The costs of publication of this article were defrayed in part by the payment of page charges. Therefore, and solely to indicate this fact, this article is hereby marked "advertisement" in accordance with 18 USC section 1734. This study was supported by the DFG (Deutsche Forschungsgemeinschaft, Grossgeräteinitiative), which funded the installation of the PET/MR scanner. No other potential conflict of interest relevant to this article was reported.

REFERENCES

1. Eiber M, Souvatzoglou M, Pickhard A, et al. Simulation of a MR-PET protocol for staging of head-and-neck cancer including Dixon MR for attenuation correction. *Eur J Radiol.* 2012;81:2658–2665.
2. Drzezga A, Souvatzoglou M, Eiber M, et al. First clinical experience with integrated whole-body PET/MR: comparison to PET/CT in patients with oncologic diagnoses. *J Nucl Med.* 2012;53:845–855.
3. Martinez-Möller A, Eiber M, Nekolla SG, et al. Workflow and scan protocol considerations for integrated whole-body PET/MRI in oncology. *J Nucl Med.* 2012;53:1415–1426.
4. Antoch G, Bockisch A. Combined PET/MRI: a new dimension in whole-body oncology imaging? *Eur J Nucl Med Mol Imaging.* 2009;36(suppl 1):S113–S120.
5. Rubens RD. Bone metastases: the clinical problem. *Eur J Cancer.* 1998;34:210–213.
6. Vanel D, Dromain C, Tardivon A. MRI of bone marrow disorders. *Eur Radiol.* 2000;10:224–229.
7. Imamura F, Kuriyama K, Seto T, et al. Detection of bone marrow metastases of small cell lung cancer with magnetic resonance imaging: early diagnosis before destruction of osseous structure and implications for staging. *Lung Cancer.* 2000;27:189–197.
8. Vanel D, Bittoun J, Tardivon A. MRI of bone metastases. *Eur Radiol.* 1998;8:1345–1351.
9. Vanel D, Casadei R, Alberghini M, Razgallah M, Busacca M, Albisinni U. MR imaging of bone metastases and choice of sequence: spin echo, in-phase gradient echo, diffusion, and contrast medium. *Semin Musculoskelet Radiol.* 2009;13:97–103.
10. Hofmann M, Pichler B, Schölkopf B, Beyer T. Towards quantitative PET/MRI: a review of MR-based attenuation correction techniques. *Eur J Nucl Med Mol Imaging.* 2009;36(suppl 1):S93–S104.
11. Hofmann M, Bezrukov I, Mantlik F, et al. MRI-based attenuation correction for whole-body PET/MRI: quantitative evaluation of segmentation- and atlas-based methods. *J Nucl Med.* 2011;52:1392–1399.
12. Schulz V, Torres-Espallardo I, Renisch S, et al. Automatic, three-segment, MR-based attenuation correction for whole-body PET/MR data. *Eur J Nucl Med Mol Imaging.* 2011;38:138–152.
13. Martinez-Möller A, Souvatzoglou M, Delso G, et al. Tissue classification as a potential approach for attenuation correction in whole-body PET/MRI: evaluation with PET/CT data. *J Nucl Med.* 2009;50:520–526.
14. Gaertner FC, Furst S, Schwaiger M. PET/MR: a paradigm shift. *Cancer Imaging.* 2013;13:36–52.
15. Delso G, Fürst S, Jakoby B, et al. Performance measurements of the Siemens mMR integrated whole-body PET/MR scanner. *J Nucl Med.* 2011;52:1914–1922.
16. Maki JH, Chenevert TL, Prince MR. The effects of incomplete breath-holding on 3D MR image quality. *J Magn Reson Imaging.* 1997;7:1132–1139.
17. Bland JM, Altman DG. Statistical methods for assessing agreement between two methods of clinical measurement. *Lancet.* 1986;1(8476):307–310.
18. Kumar J, Seith A, Kumar A, et al. Whole-body MR imaging with the use of parallel imaging for detection of skeletal metastases in pediatric patients with small-cell neoplasms: comparison with skeletal scintigraphy and FDG PET/CT. *Pediatr Radiol.* 2008;38:953–962.
19. Schmidt GP, Schoenberg SO, Schmid R, et al. Screening for bone metastases: whole-body MRI using a 32-channel system versus dual-modality PET-CT. *Eur Radiol.* 2007;17:939–949.
20. Eiber M, Martinez-Möller A, Souvatzoglou M, et al. Value of a Dixon-based MR/PET attenuation correction sequence for the localization and evaluation of PET-positive lesions. *Eur J Nucl Med Mol Imaging.* 2011;38:1691–1701.
21. Samarin A, Burger C, Wollenweber S, et al. PET/MR imaging of bone lesions: implications for PET quantification from imperfect attenuation correction. *Eur J Nucl Med Mol Imaging.* 2012;39:1154–1160.
22. Souvatzoglou M, Ziegler SI, Martinez MJ, et al. Standardised uptake values from PET/CT images: comparison with conventional attenuation-corrected PET. *Eur J Nucl Med Mol Imaging.* 2007;34:405–412.
23. Nakamoto Y, Osman M, Cohade C, et al. PET/CT: comparison of quantitative tracer uptake between germanium and CT transmission attenuation-corrected images. *J Nucl Med.* 2002;43:1137–1143.
24. Kumar R, Loving VA, Chauhan A, Zhuang H, Mitchell S, Alavi A. Potential of dual-time-point imaging to improve breast cancer diagnosis with ^{18}F-FDG PET. *J Nucl Med.* 2005;46:1819–1824.
25. Schirrmeister H. Detection of bone metastases in breast cancer by positron emission tomography. *Radiol Clin North Am.* 2007;45:669–676.
26. Cook GJ, Houston S, Rubens R, Maisey MN, Fogelman I. Detection of bone metastases in breast cancer by ^{18}FDG PET: differing metabolic activity in osteoblastic and osteolytic lesions. *J Clin Oncol.* 1998;16:3375–3379.

JNM The Journal of NUCLEAR MEDICINE

Performance of Whole-Body Integrated ^{18}F-FDG PET/MR in Comparison to PET/CT for Evaluation of Malignant Bone Lesions

Matthias Eiber, Toshiki Takei, Michael Souvatzoglou, Marius E. Mayerhoefer, Sebastian Fürst, Florian C. Gaertner, Denys J. Loeffelbein, Ernst J. Rummeny, Sibylle I. Ziegler, Markus Schwaiger and Ambros J. Beer

J Nucl Med. 2014;55:191-197.
Published online: December 5, 2013.
Doi: 10.2967/jnumed.113.123646

The Journal of Nuclear Medicine is published monthly.
SNMMI | Society of Nuclear Medicine and Molecular Imaging
1850 Samuel Morse Drive, Reston, VA 20190.
(Print ISSN: 0161-5505, Online ISSN: 2159-662X)

SNMMI SOCIETY OF NUCLEAR MEDICINE AND MOLECULAR IMAGING